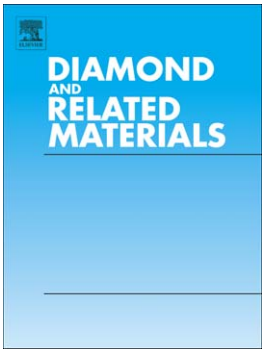

Nano-carbon pixels array for ionizing particles monitoring

S. Salvatori, P. Oliva, M. Pacilli, P. Allegrini, G. Conte, M. Komlenok, A.A. Khomich, A. Bolshakov, V. Ralchenko, V. Konov

PII: S0925-9635(16)30275-8
DOI: doi: 10.1016/j.diamond.2016.08.011
Reference: DIAMAT 6688

To appear in: *Diamond & Related Materials*

Received date: 30 June 2016
Accepted date: 23 August 2016

Please cite this article as: S. Salvatori, P. Oliva, M. Pacilli, P. Allegrini, G. Conte, M. Komlenok, A.A. Khomich, A. Bolshakov, V. Ralchenko, V. Konov, Nano-carbon pixels array for ionizing particles monitoring, *Diamond & Related Materials* (2016), doi: 10.1016/j.diamond.2016.08.011

Nano-carbon pixels array for ionizing particles monitoring

S. Salvatori [a], P. Oliva [a,b]

[a]*Niccolò Cusano University, Via don Carlo Gnocchi, 3 – 00166 Rome, Italy*

[b]*Mediterranean Institute of Fundamental Physics 'MIFP', Via Appia Nuova, 31 – 00040 Marino (Rome), Italy*

M. Pacilli [c], P. Allegrini [c], G. Conte [c],

[c]*Department of Sciences, University Roma Tre, Via della Vasca Navale, 84 – 00154 Rome, Italy*

M. Komlenok [d], A.A. Khomich [d], A. Bolshakov [d], V. Ralchenko [d], V. Konov [d]

[d]*A.M. Prokorhov General Physics Institute, Russian Academy of Sciences*

38 Vavilova Str. – 119991 Moscow, Russia

Abstract

The paper deals on the response of a polycrystalline diamond sensor, 500 μm thick, to particles from a ^{90}Sr β-source. 21×21 nano-carbon pads, with 0.18 mm×0.18 mm area each, were realized by ArF excimer laser irradiation on one diamond face, whereas a 7×7 mm^2 backside contact was fabricated and used for sensor biasing during characterization of sensor under β-source irradiation. The carbon pads embrace a number of grains, which show different degrees of surface graphitization dependent on the grain orientations. Each carbon pad exhibits a linear I(V) response up to 200 V. The average number of charge carriers collected by a single pixel, as well as the distribution of pixels involved by the impinging particle tracking, is analyzed as a function of the applied voltage recording the signals acquired by 16 pixels at a time. The pulse height distribution is not affected by reversing the bias polarity. For a single pixel, the most probable collected charge value is 1.40±0.02 fC whereas the main value gives $<Q>_{coll}$=1.67±0.02 fC (10430 ±120 electrons). The charge collection distance was measured tacking into account the effect induced by high-energy electrons and found to be 285±3 μm, demonstrating the absence of bulk defects induced by the laser graphitization processing. Cross-talk effects between nearest-neighbor pixels has been excluded analyzing the results obtained in a batch of more than 1000 events even if the same cannot be excluded under higher energy particles.

1. Introduction

One- and two-dimensional pixel array detectors are able to give information on both the beam position and the beam intensity profile of the impinging radiation. Even if a pixelated sensor may show a relatively high device cost, also induced by a more complex front-end electronics to be connected to each pixel, a detector made from an array of discrete sensing elements (*i.e.* photo-resistors or photo-diodes) shows several advantages if compared to other detectors [1, 2]. When ionizing particles are concerned, pixel detectors are also effective to resolve the position of the impinging radiation. In such a field, poly-crystalline diamond specimens have shown their suitability [3, 4]. The design of small area pixels, aimed to obtain low capacitance and a corresponding lower electronic noise amplitude, also reduces cross-talk effects between monitored signals from nearest neighbor pixels. Such features become extremely relevant in designing the processes involved in excimer laser treatment techniques used to define the active area of small tight pixels on the synthetic polycrystalline diamond [5-7].

While diamond represents a robust dielectric, under proper conditions, laser induced graphite or nano-carbon aggregates on diamond surface exhibit a strong adhesion to underneath bulk and also allow to realize electric contacts having a high conductance. However, the same optimal conditions could also produce electronic active defects in the region between adjacent pads, reducing the possibility to realize a detector having a high pixel density.

In a previous paper [4], we reported the study of a polycrystalline CVD-diamond based sensor composed of an array of 6×6 graphite pixels, 1 mm×1 mm wide, fabricated by using a 248 nm KrF excimer laser irradiation. While the use of a 248 nm laser light involves the absorption towards sub-gap diamond states, phonon-assisted processes are involved when an over bandgap 193 nm laser source is concerned. In such a case the graphitization efficiency will be also dependent on the

diamond grain orientation [8], which also affects material ablation and surface damage. Ablation and surface damage, as well as the threshold energy at different wavelength, has been analyzed by J. Smedley *et al.* [9] addressing weaker radiation laser light intensity to produce most uniform and less defected surfaces.

In this work we report the fabrication and test of a new 21×21 pixel array diamond detector. Each pixel, realized by means of a 193 nm ArF excimer laser, has 180×180 μm^2 area. Tests have been performed in order to demonstrate that the sensor is able to monitor β-particles emitted from a ^{90}Sr radioactive source, showing a high signal discrimination between nearest neighbor pixels and that it can be moved toward particle tracking.

2. Experimental issues

2.1 Material and laser treatment setup

The diamond sample used in this work was a commercial CVD polycrystalline diamond plate, produced by Element Six [10], having a 10 mm×10 mm×0.5 mm size, for which both the two diamond sides were mechanically polished by the manufacturer reducing the sample surface roughness to about 4 nm. The diamond slab was dipped in boiling $K_2Cr_2O_7$ saturated H_2SO_4 (sulphochromic) acid mixture and rinsed in aqua regia, $HCl:HNO_3$ (3:1), mixture in order to remove any chromium residuals [11, 12]. Finally, the sample was cleaned in deionized water and isopropyl alcohol. Such a process aims to remove any conductive path from the sample surface. The diamond plate was then fixed on a motorized stage so that its nucleation side was irradiated by a pulsed UV ArF excimer laser (λ=193 nm, τ=20 ns, CL7100 model, Optosystems Ltd). The UV laser light beam was focused to obtain an illuminating spot having a dimension of 180 µm×180 µm on the diamond surface, thus defining the graphitic pixel size. A squared guard ring contact (180 µm wide), surrounding the pixel array, to be connected to the same pixels potential, was also fabricated

shifting the laser spot by 100 µm, allowing for a drastic decrease of the leakage current contribution from the defected diamond sample edges.

The laser light intensity on the sample surface was around 6 $J \cdot cm^{-2}$, well above the surface graphitization threshold of ≈ 2 J/cm^2 [13]. The crystallites with typical size of 10-20 µm are observed on the nucleation side of CVD-diamond (figure 1). The computer-controlled translation stage allowed to realize an array composed by 21×21 pixels, 120 µm apart along both the orthogonal directions, on the diamond nucleation side. Three consecutive laser pulses have been used to irradiate the same area to be treated.

The initial average surface roughness increased from 4 nm to 30 nm as a result of the graphitization treatment which is also accompanied by material ablation. The average thickness of the laser induced graphitized layer has been evaluated to be of about 120 nm, as measured by means of an optical profiler of a test pixel before and after chemical etching in hot sulphochromic acid mixture able to remove any graphitic specimens [11].

The Raman spectra of diamond samples taken at an excitation wavelength of 488 nm (LabRAM HR800, Horiba) after laser irradiation with the fluence above graphitization threshold usually reveal the diamond peak at 1332.5 cm^{-1} and two broad peaks around 1360 cm^{-1} (D band) and 1580 cm^{-1} (G band) assigned to disordered carbon or nano-graphite [14, 15]. However, in our case intensities of these bands rather differ from one grain to another as illustrated by figure 2. The optical micrograph also reports a spotty pattern (figure 1) in which each crystallite exhibits a different blackness degree due to difference in local thickness of the graphite layer, in sp^3/sp^2 ratio and, possibly, in surface roughness.

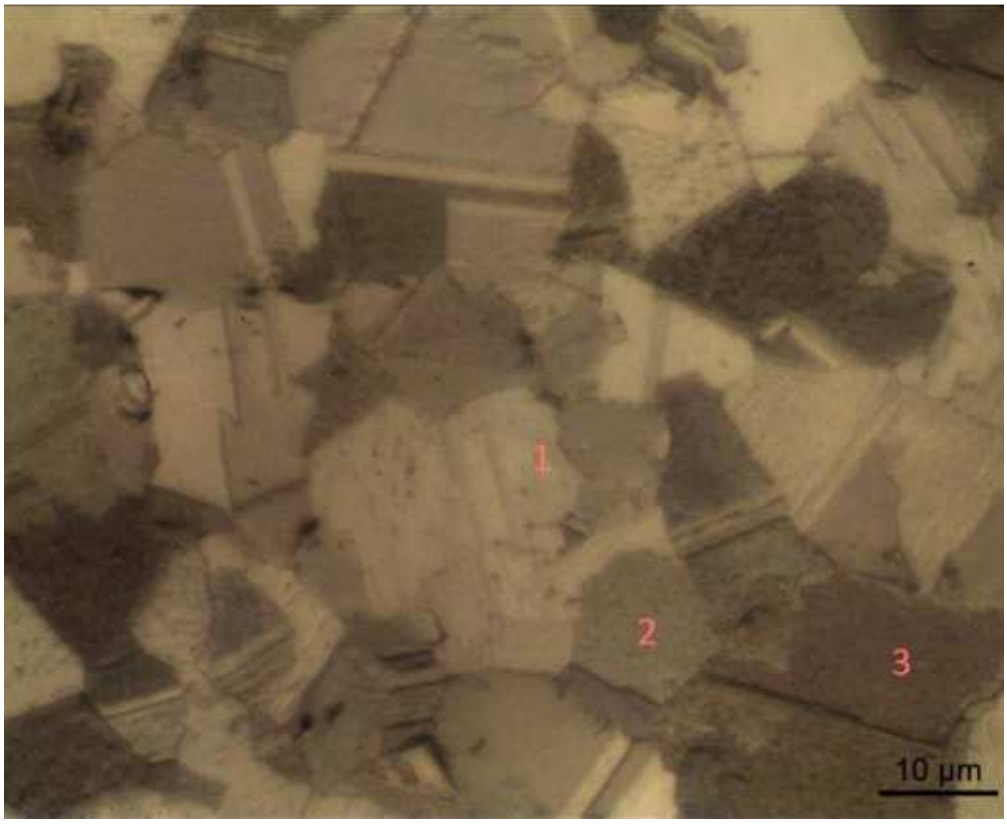

Figure 1. A part of 180 µm×180 µm pixel formed by laser irradiation on the nucleation side of the diamond plate (optical micrograph in reflection). Note a patchwork optical contrast picture of the surface due to the dependence of graphitization rate on grain orientation. Raman spectra for the grains #1, 2 and 3 with essentially different optical contrast are compared in figure 2.

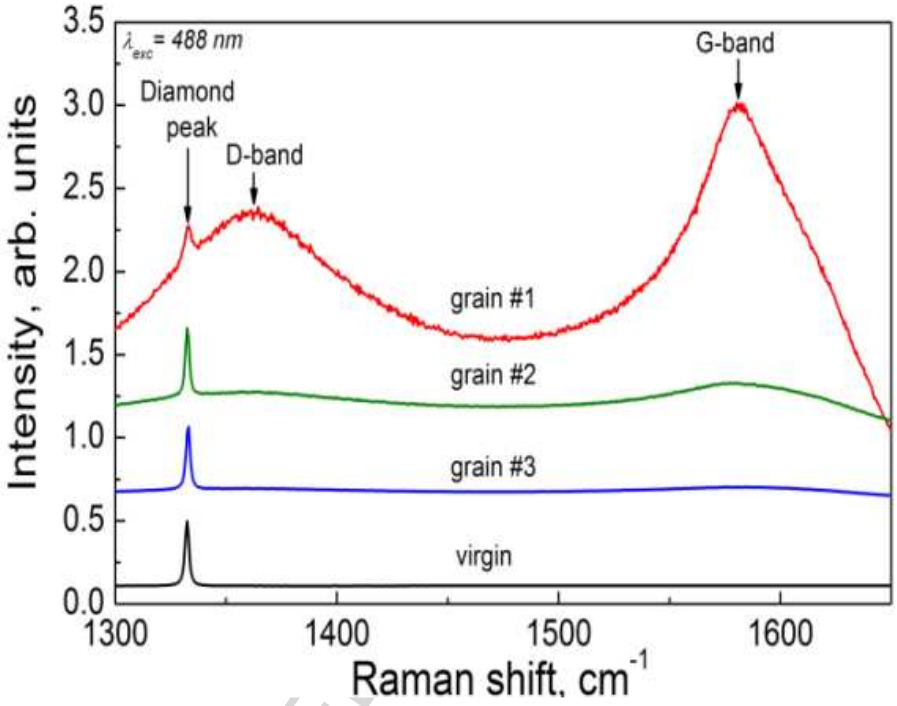

Figure 2. Raman spectra taken in three different locations (on grains #1, 2 and 3 in figure 1) within the same graphitic pixel as compared with the spectrum of virgin diamond (bottom spectrum). All spectra normalized to the diamond peak intensity.

This variation occurs due to difference in graphitization rate for different diamond crystallographic planes as known from experiments on thermal annealing of single crystal diamonds [16]. Thicker graphitic layers look brighter due to higher reflectivity of the graphite as compared to diamond. Thus, the graphite thickness (and, as a consequence, the electrical resistance of the contact) for each pixel has actually resulted as an average quantity for about the 300 grains (each with its own thickness of graphite layer determined by the grain orientation) included within a single pixel. In addition, also note that Raman spectrum of non-treated area is similar to that named "virgin" in Figure 2 in which only the 1332 cm^{-1} diamond peak is observed.

2.2 Measurement setup

To host the matrix and the hybrid charge sensitive pre-amplifiers we used a low-noise printed circuit board (PCB). A large back graphite contact was used to attach the sample to the PCB with carbon dag. Conversely, individual pixels were wire bonded towards the amplifier inputs.

Two more slabs, 1 cm^2 large, of electronic grade polycrystalline diamond by Element Six, were coated with 8×8 mm^2 sputtered silver contacts (defined by means of a metal mask), 100 nm thick, and glued on independent low-noise PCB supports, with their own pre-amplifier, power supply and calibration signal input. Such two large area detectors were used to produce trigger signals in order to monitor a particle passage. The charge sensitive pre-amplifier are based on CAEN A1422H-F2, 45 mV/MeV(Si) components with an input test capacitance C_{test} = 1 pF. Solid state batteries were used for low voltage ±12 V front-end amplifier power supply. A CAEN N1471A power supply was used to apply the bias voltage to the matrix using the large backside graphite pad, while an Ortec-556 2-channels power supply was used for front and back triggers. A group of 4×4 pixels was wire bonded with Al/Si standard 25 µm wires directly on the graphite pads for testing. The wire diameter used for bonding is thin enough to avoid particle's energy attenuation. The charge collection was

analyzed under un-collimated 1 MBq ^{90}Sr,Y test source [17], 1 mm in diameter, hold 2 cm apart from the front trigger. The ^{90}Sr radioactive source produces electrons with continuous energy β^- decay spectrum. ^{90}Sr decays by β^- emission to ^{90}Y with end-point energy 0.53 MeV, then new β^- decay to ^{90}Zr are observed with end-point kinetic energy 2.28 MeV. For electrons with kinetic energy of 0.5 MeV, the energy loss in a 500 μm diamond film is approximately $\Delta E \sim 0.35$ MeV. Thus, electrons with energy below 0.5 MeV will stop in the front trigger diamond film, located 5 mm apart the pixelated matrix. On the other hand, electrons with kinetic energy above 1.2 MeV behave resembling MIPs (Minimum Ionizing Particles) producing 36 e-h/μm. Two synchronized CAEN V1724 8-channels digitizers 14 bits, 100 MS/s and 500 mV_{pp} of dynamic range were used together with CAEN N6724a 2-channels, 14 bits, 100 MS/s and 500 mV_{pp} of dynamic range for triggers signal. This instrument was equipped with digital pulse height analysis firmware. The acquisition and data dumping starts when a coincidence signal on the two triggers – about 1.5 cm apart – is revealed. The coincidence time window, as the acquisition time period, was optimized in order to reduce data dumping without time resolution lost. Acquisition and *ex-situ* traces elaboration were carried out by using dedicated C^{++}/Fortran programs. In order to evaluate the average charge collected by each pixel, a calibration curve was prepared by means of pulses generated from an Agilent 33250A waveform source generator with pre-programmed rise- and decay-time and amplitude of built-in curves.

3. Results and Discussion

3.1 Single pixel charge collection

Initially, aimed to evaluate the charge collected by a single pixel, we used a self-triggering acquisition mode to monitor the pixel signal dependence on the applied bias voltage. Figure 3 shows the distribution of measured events (PHD) versus the collected charge of a pixel as a function of the negative bias voltage. It is worth to note that the spectra have been produced without any filtering effect of the front trigger.

Figure inspection depicts a well resolved β-source spectrum, with a clear separation from the unavoidable noise contribution. The distribution most probable value (MPV) shows a saturation effect around -300 V (0.6 V/μm).

Table I reports the MPV value as well as the average collected charge $<Q>_{coll}$ of the measured PHD at different bias voltages. Reversing the applied bias voltage, the charge collection appears to be symmetric. If we compare such results with those of a 1 mm^2 large graphite pixel reported in [4], an interesting indication is derived: in the case of 1 mm^2 large pixel, a saturation of collected charges was observed at the value $<Q>_{coll}$ = 1.71±0.02 fC (~10700 electrons); conversely, for a pixel 25 times smaller, we now observe a saturation value quite similar to that obtained for larger pads and equal to $<Q>_{coll}$=1.67±0.02 fC (10430±120 electrons). Such a result states that no-loss of charge carriers is observed decreasing the pad area, at least at the tested applied voltage, so that their collection only depends on particle path length.

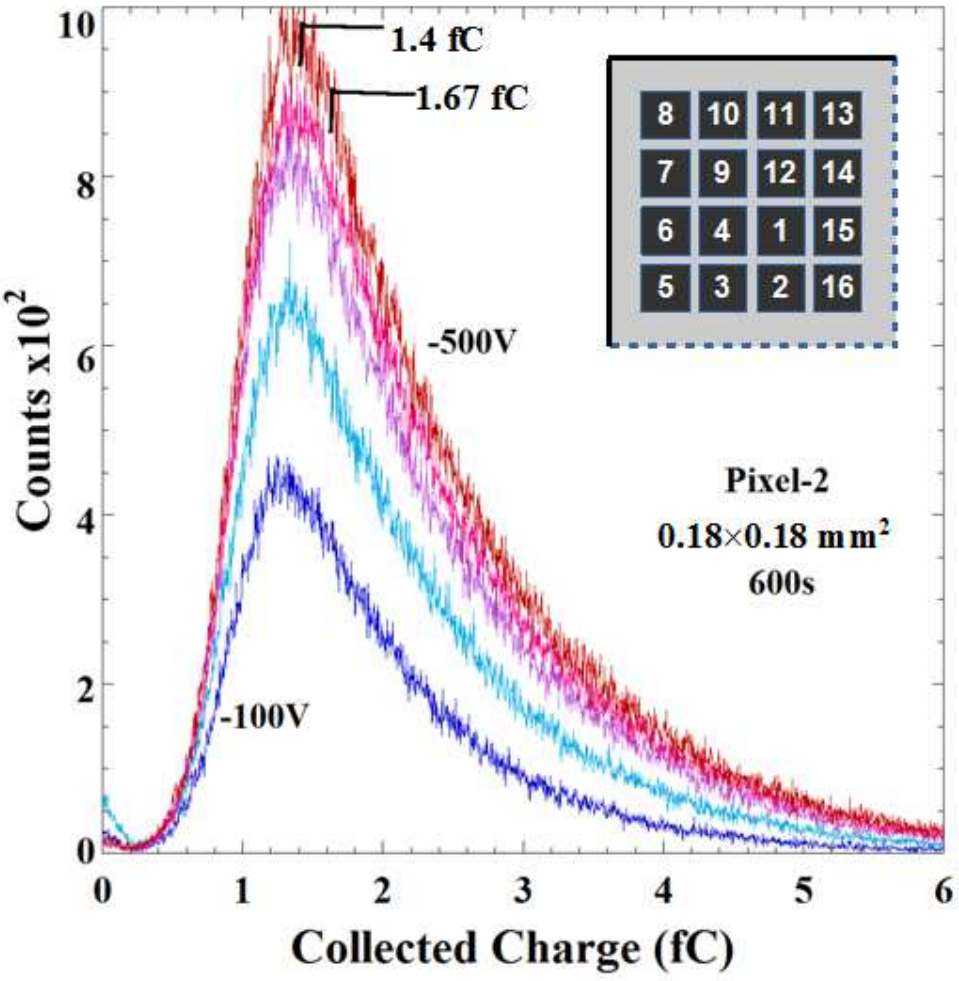

Figure 3. Pixel n.2 signal dependence at different negative voltage biasing. Most probable and mean charge collection values are indicated on the top. The inset depicts the labeling of the 16 pixels (according to wire bonded input front-end amplifiers).

Table I. Charge collection on pixel n. 2.

Bias (V)	**MPV (fC)**	**<Q> (fC)**
-100	1.30	1.63
-200	1.34	1.64
-300	1.36	1.65
-400	1.39	1.66
-500	1.40	1.67
500	1.41	1.68
400	1.38	1.66
300	1.36	1.65
200	1.32	1.63

3.2 Charge collection efficiency

Following the method described in [4], a coincidence acquisition mode has been used to estimate the charge collection efficiency (CCE) gained at each pixel. For the sensor thickness of 500 μm, a Q_{gen} = 36×500 μm = 18000 electrons number is expected on the charge carriers generation. It has to be observed that the front trigger, made from a polycrystalline diamond slab, was also able to filter-out any low-energy electrons contribution. Such a characterization was also devoted to infer possible detrimental effects due to the laser writing process, potentially affecting the charge collection efficiency of the realized pads.

The collected charge mean value has been evaluated from the PHD measurements performed at 400 V (0.8 V/μm) as that reported in figure 4. A MPV = 1.40±0.02 fC and a $\langle Q \rangle_{coll}$ = 1.67±0.02 fC (10430±120 electrons) are evaluated, with 99% of the distribution above 6000 electrons.

Being the charge collection efficiency given by the ratio

$$CCE = \frac{<Q>_{coll}}{Q_{gen}} \quad (1)$$

a CCE = 0.57±0.01 value is calculated for data reported in figure 4. Such a quantity corresponds to a charge collection distance equal to 285±3 μm (CCE times the sensor thickness), a value in good agreement with what found for best quality polycrystalline diamond samples [18] and demonstrating the absence of any bulk defects induced by the ArF laser treatment used for pads realization. Indeed, it has been reported that during graphitization with *ns* pulsed lasers some defects can be created at the diamond/graphite interface [19] possibly resulting in a charge carriers loss and a corresponding CCE decrease.

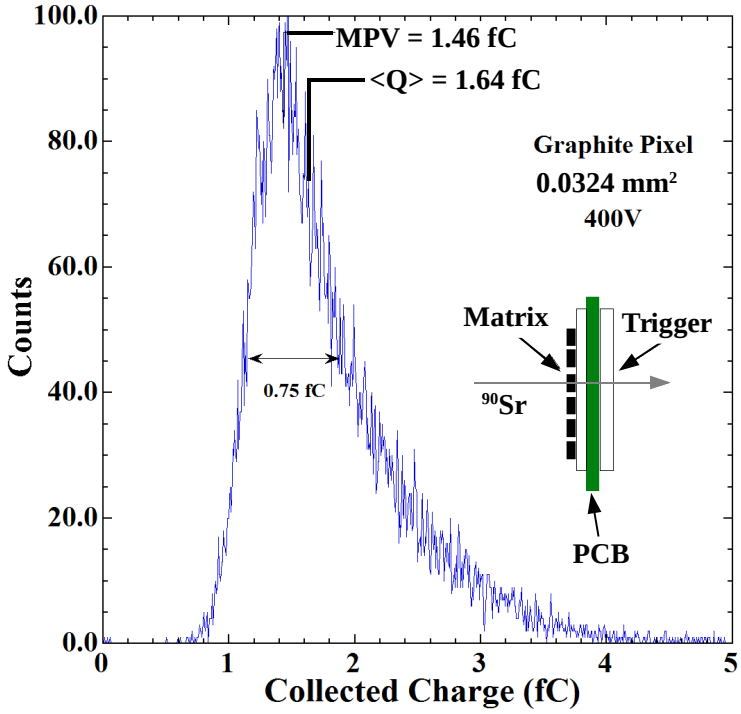

Figure 4. PHD of the pixel n.1 measured in coincidence with the back trigger. To filter low-energy electrons was used the front trigger as described in [20].

3.3 Cross-talk analysis

Once confirmed the good quality of the fabricated matrix, we carried out sensor characterization by coincidence mode acquisition and analysis using the output signals generated by both the front- and the back-trigger at the β-particle passage to download the 16 traces data taken by means of the two V1724 digitizers. By such a method, the β-particle impinging point on the diamond surface can be easily estimated analyzing the trace signals recorded at each pixel and evaluating the pixels involved in charge carriers collection.

Figure 5 reports an example of eight traces recorded by one of the two V1724 digitizers used during the measurements. As highlighted by traces behavior reported in the figure, only the pixel n. 2 has been involved on the charge carrier collection. The step amplitude shown by such a trace corresponds to about 4.0 fC (~25000 electrons). If we refer to the previous data of figure 3, this transition corresponds to a high energy event associated with the PHD long exponential tail.

To evaluate how the system allows to discriminate small step amplitudes, signal distribution of trace "2" of figure 5 is reported in figure 6. Here, the average initial ADC channel 8765 value has been considered as reference and subtracted for a clearer view. The standard deviation of the signal trace corresponds to 3.58±0.06 ADC channels underlining the possibility to discriminate steps larger than 5 ADC channels (*i.e.* ~0.5 fC, ~3000 electrons) and also confirmed by inspection of the data reported in figure 4. Such a result is quite representative of all the 16 channels, although higher noise has been sometime observed at the highest voltage values used for sensor biasing.

Figure 7 shows the case in which a particle involves four nearest neighbor pixels in the charge carrier collection: 1, 12, 14, and 15. The step amplitude of pixel "14" is the largest (25 ADC channels) in comparison to that of the other pixels. Adding the four step quantities we obtain a total of 51 ADC involved channels (*i.e.* 4.8 fC) and related to a relative high energy particle. The result here reported seems to indicate the possibility to detect the passage of a particle in the median point of the four nearest neighbor pixels only when a high energy particle is concerned.

Finally, figure 8 reports the distributions of the pixels involved (cluster dimension) by 1100 impinging β-particle events. The data have been acquired with the matrix biased at 300 V and using 100 V for both the two triggers. More than 80% of the events involved a single pixel, whereas 14% related to two pixels, and only 3% three pixels. The residual 1% of events concerned four pixels. The observed decreasing trend in this representative batch agrees with statistical rules on non-interacting events. The histogram also highlights that only one pixel is generally switched-on. Therefore, cross-talk effects, as charge sharing between pixels, cannot be excluded because of the low-energy of particles from the ^{90}Sr β-source used during sensor characterization. Tests with high-energy electrons are mandatory to advance conclusions on the suitability of such a nano-graphite array of pixels for particle tracking.

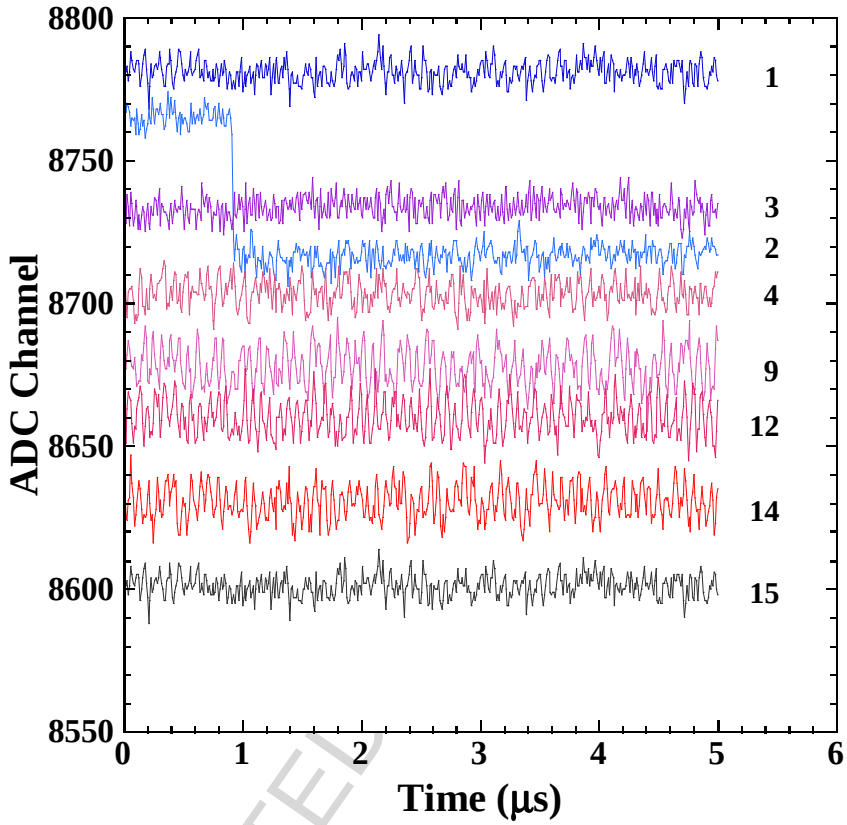

Figure 5. Eight of the nine traces from one V1724 digitizer. All traces are around the central pixel n.1 that, in this case, has not switched-on.

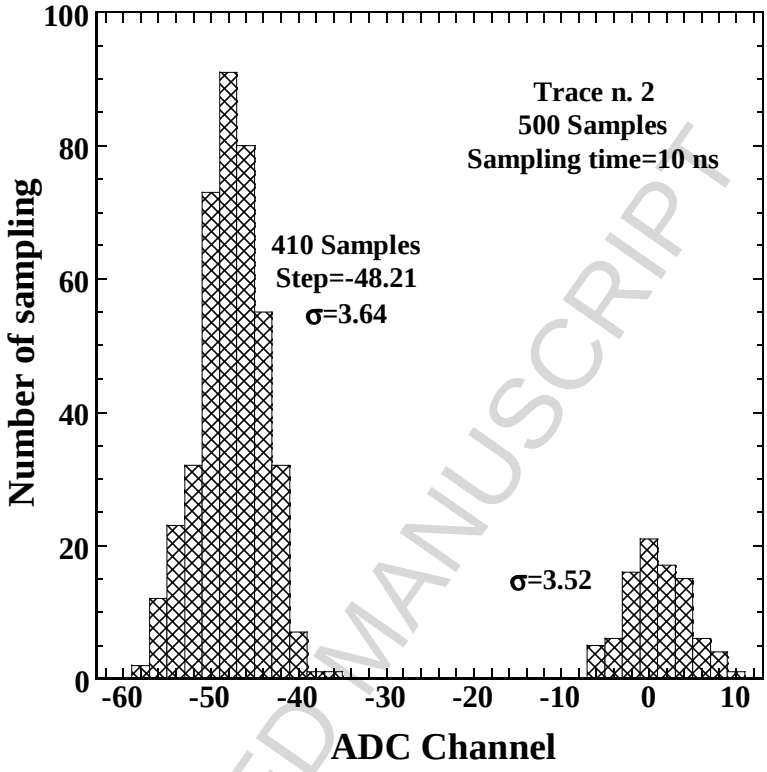

Figure 6. Statistical distribution of the trace signal of figure 5 at pixel n.2 in. The average ADC channel number before particle detection has been subtracted for a better representation and analysis. The bin size is equal to 2 channels.

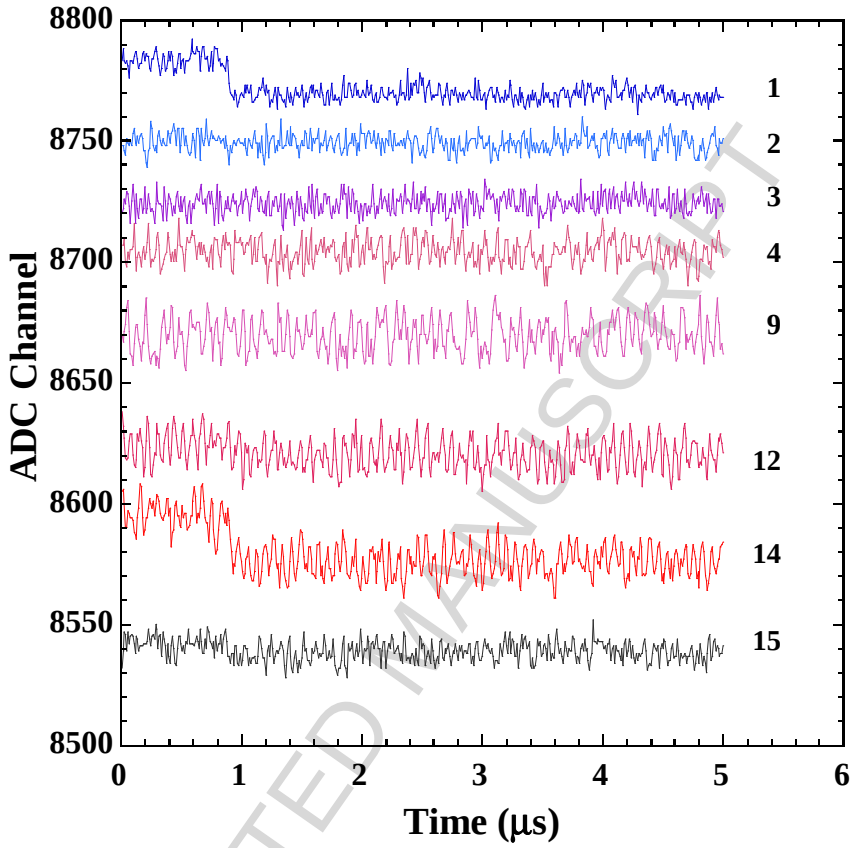

Figure 7. Traces from one V1724 8-channels digitizer. All traces are around the central pixel n.1 that has been switched-on together with number 12, 14 and 15.

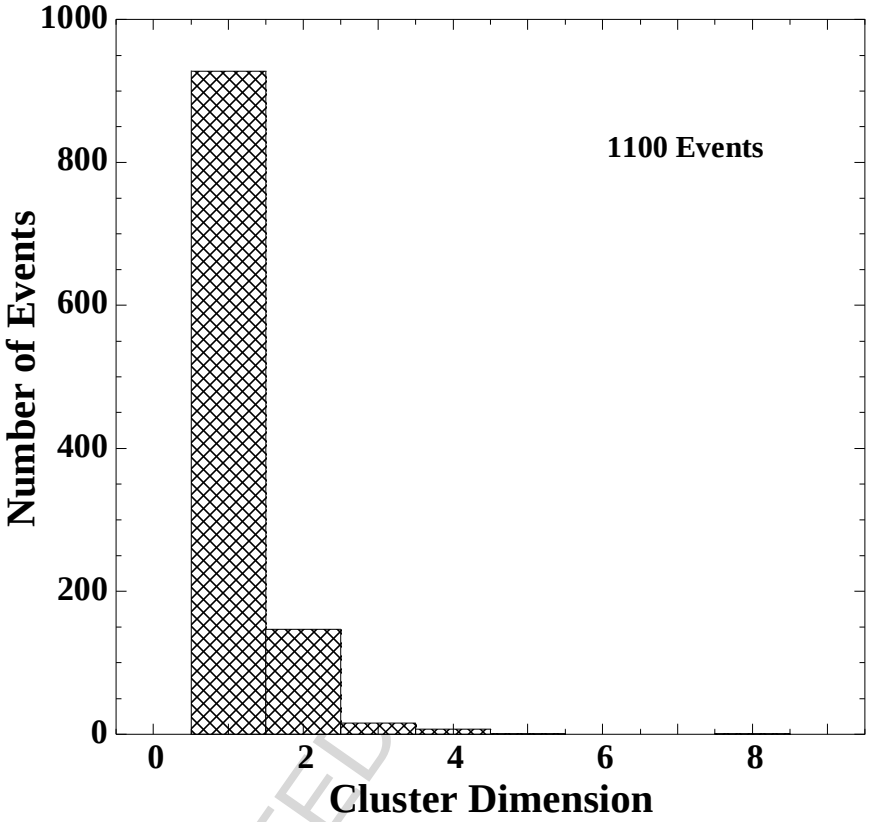

Figure 8. Number of pixels (cluster) distribution resulting from the analysis of a batch of 1100 events with the matrix biased at 300V and the two triggers at 100V.

4. Concluding remarks

The feasibility of a pixel-array detector based on high-quality CVD-diamond to be used for low-energy β-particles monitoring has been shown. Experimental results highlight that no-loss of collected charges is observed decreasing the pixel area, estimating a charge collection distance of about 290 μm, a value usually found in very good quality samples as that used in this work. Cross-talk between adjacent pixels has not been revealed under ^{90}Sr β-source irradiation, even if further investigation under higher energy particles has to be carried out. However, the results here reported move toward the possible realization of high-density pixel diamond sensors, where pads are realized by laser treatment of diamond surface in order to obtain an all-carbon detector able to remove any loss due to metal contacts absorption of impinging particles.

Acknowledgements

A part of this work on laser-assisted graphitic contacts formation was performed with financial support of Ministry of Education and Science of Russian Federation, Agreement No. 14.579.21.0030, the unique identifier RFMEFI57914X0030.

References

[1] G. Bertuccio, Prospect for energy resolving X-ray imaging with compound semiconductor pixel detectors, *Nucl. Instr. and Meth. in Physics Research Section A* 546 (2005) 232-241.

[2] M. Girolami, P. Allegrini, G. Conte, S. Salvatori, D. M. Trucchi, A. Bolshakov, V. Ralchenko, Diamond Detectors for UV and X-Ray Source Imaging, *IEEE-EDL* 33 (2012) 224-226.

[3] H. Kagan, Recent advances in diamond detector development, *Nucl. Instr. and Meth.in Physics Research Section A*, 541 (2005) 221-227.

[4] M. Pacilli, P. Allegrini, G. Conte, E. Spitriti, V. Ralchenko, M. Komlenok, A. Bolshakov, A.A. Khomich, V. Konov, Beta particles sensitivity of an all-carbon detector, *Nucl. Instr. Meth. in Physics Research Section A*, 738 (2014) 119-125.

[5] S.M. Pimenov, G.A. Shafeev, V.A. Laptev, E.N. Loubnin, Laser activation of diamond surface for electroless metal plating, *Appl. Phys. Lett.* 64 (1994) 1935-1937.

[6] T.V. Kononenko, V.V. Kononenko, V.I. Konov, S.M. Pimenov, S.V. Garnov, A.V. Tishchenko, A.M. Prokhorov, A.V. Khomich, Formation of antireflective surface structures on diamond films by laser patterning, *Appl. Phys. A: Materials Science & Processing* 68(1) (1999) 99-102.

[7] M. Pacilli, P. Allegrini, M. Girolami, G. Conte, E. Spiriti, V.G. Ralchenko, M.S. Komlenok, A.A. Khomich, V.I. Konov, Polycrystalline CVD diamond pixel array detector for nuclear particles monitoring, *Journal of Instrumentation* 8 (2013) C02043.

[8] R.A. Khmelnitsky, A.A. Gippius, Transformation of diamond to graphite under heat treatment at low pressure, *Phase Transitions* 87 (2014) 175-192.

[9] J. Smedley, J. Bohon, Q. Wu, T. Rao, Laser patterning of diamond. Part I. Characterization of surface morphology, *J. Appl. Phys.* 105 (2009) 123107.

[10] Element Six Technologies, www.e6.com.

[11] S. Salvatori, A. Della Scala, M. C. Rossi, G. Conte, Optimised contact-structures for metal–diamond–metal UV-detectors, *Diamond and Relat. Mater*. 11 (2002) 458-462.

[12] M. C. Rossi, F. Spaziani, S. Salvatori, G. Conte, Electronic properties of hydrogen and oxygen terminated surfaces of polycrystalline diamond films, *Phys. Stat. Sol. (a)* 199 (2003) 71-76.

[13] H. Suzuki, M. Yoshikawa, H. Tokura, "*Excimer laser processing of diamond films*", in: S. Saito et al (Eds.), *Advances in New Diamond Science and technology*, MYU, Tokyo, 1994, pp. 501-504.

[14] P. Lespade, R. Aljishi, M. S. Dresselhaus, Model for Raman scattering from incompletely graphitized carbons, *Carbon* 20 (1982) 427-431.

[15] S. Prawer, K. W. Nugent, Y. Lifshitz, G. D. Lempert, E. Grossman, J. Kulik, I. Avigal, R. Kalish, Systematic variation of the Raman spectra of DLC films as a function of sp^2:sp^3 composition, *Diamond and Relat. Mater*. 5 (1996) 433-438.

[16] T. Evans, "*Changes produced by high temperature treatment of diamond*", in: J.E. Field, ed., *The Properties of Diamond*, Academic Press, London, 1979, p. 403.

[17] QSA Global, code SIFB13505, item 22/2006.

[18] W. Adam, *et al.*, Development of Diamond Tracking Detectors for High Luminosity Experiments at the LHC, CERN/LHCC 2006-010, LHCC-RD-010, Status Report/RD42, March 1, 2006.

[19] V. I. Konov, T. V. Kononenko, V.V. Kononenko, *Laser Micro- and Nanoprocessing of Diamond Materials*, in: R.P. Mildren and J.R. Rabeau (Eds.), Optical Engineering of Diamond, Wiley-VCH Verlag GmbH & Co. KgaA, 2013, pp 385–443; ISBN 9783527648603.

[20] G. Conte, P. Allegrini, M. Pacilli, S. Salvatori, T. Kononenko, A. Bolshakov, V. Ralchenko, V. Konov, Three-dimensional graphite electrodes in CVD single crystal diamond detectors: Charge collection dependence on impinging β-particles geometry, *Nucl. Instr. Meth. in Physics Research Section A* 799 (2015) 10-16.

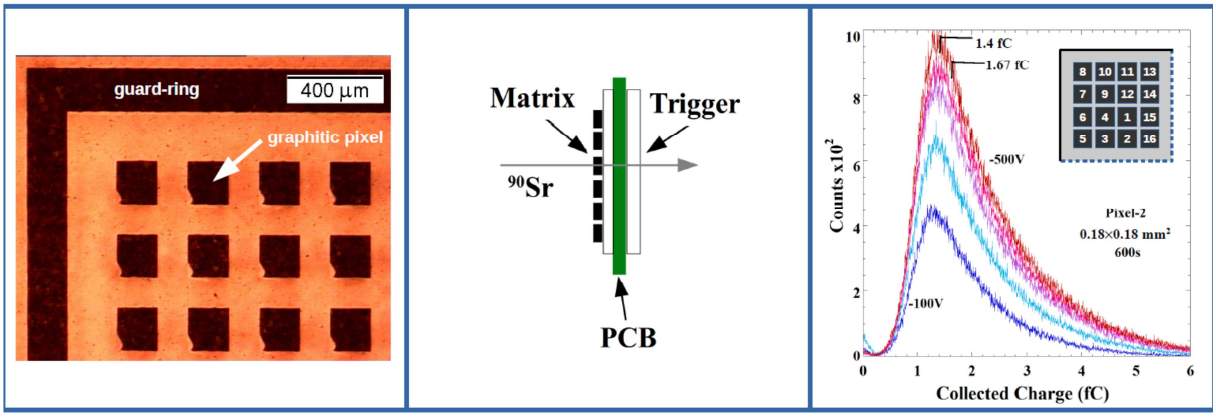

Graphical abstract

Highlights

1. An all-carbon based pixelated-pads particle-detector is presented.

2. Surface 193 nm laser light polycrystalline diamond graphitization has been performed.

3. Coincidence analysis using two more polycrystalline diamond triggers was adopted.

4. Complete charge collection at 300 V (saturation voltage amplitude) has been found.

5. No cross-talk effects between nearest-neighbor pixels (880/cm^2) have been observed.